Controlled Generation of TiO_x-Au interface using Titanium Molecular Complex Bearing Pyridyl Anchors – Synthesis, Characterization and Catalysis

Zhen Wang,[a,b,%] Xianliang Hou,[c,†] Yi Y. Wu, [b,†] Jingmei Shen,[b] Tiehu Li,[c] Changqing Fang,[a] Mayfair C. Kung,[b,*] and Harold H. Kung,[b,*]

[a] *Faculty of Printing, Packaging Engineering and Digital Media Technology, Xi'an University of Technology, Xi'an, 710048, P. R. China*
[b] *Chemical and Biological Engineering Department, Northwestern University, Evanston, IL 60208, USA*
[c] *School of Materials Science and Engineering, Northwestern Polytechnical University, Xi'an, Shaanxi 710072, P. R. China*

[%] *Experimental work were conducted at Northwestern University.*

[†] *X. Hou and Y. Wu contributed equally in this work.*

**Corresponding authors:m-kung@northwestern.edu, hkung@northwestern.edu*

Keyword: inverse catalyst; supported gold; interface; TiO_x; propane oxidation; titanium complex precursors.

Abstract

Interfacial perimeter sites between metal and support are often important for catalysis. A mononuclear titanium siloxy complex **III**, $Ti(acac)_2[OSiC_6H_5N(OCH_3)_2]_2$ was synthesized to generate TiO_x units of different degrees of clustering to decorate Au nanoparticles. Two different methods of preparation were examined; one was to deposit **III** onto Au/SiO_2 and the other was to form **III**-covered Au nanoparticle first before deposition onto SiO_2. The former method generated more highly dispersed TiO_x units, while larger domains of TiO_2 were formed with the latter method, as deduced by UV-vis and XAS characterization. A model was proposed to explain how TiO_x dispersity could be related to the preparative procedures. These samples were further tested as catalysts in selective oxidation of propane in a stream of O_2 and H_2. They exhibited different product selectivities. The sample with more dispersed TiO_x units were more selective for acetone formation versus propene formation. The results confirmed the important role of both the Au-TiO_x interface at the perimeter and the extent of Ti isolation in the TiO_x phase in the reaction.

I. Introduction

The activity of metal catalysts often strongly depends on the nature of the support oxide. This dependence is particularly noticeable for Au-based catalysts. The strong dependence of CO oxidation activity on both Au particle size and the nature of the support led Bond and Thompson to propose that the active site for CO oxidation resides at the perimeter between Au and the support.[1] Subsequently, strong evidence began to appear to support the importance of the interfacial perimeter sites in Au catalysis.[2-7]

An interesting approach in studying interfacial perimeter sites is the construction of a model inverse catalyst, whereby metal oxide is deposited onto a metal film. Applying this approach to various metals, it was found that the perimeter sites are important in oxidation catalysis over metallic systems such as Pt[8, 9] and Cu,[10] in addition to Au. Thus, controlled synthesis of tailored metal oxide around catalytic metal active sites is paramount in gaining insight and understanding of supported metal catalysts.

Since Au catalysis may be particle size dependent,[11, 12] inverse catalysts constructed with metal nanoparticles instead of films may be more representative of supported catalysts. Our initial investigation into the synthesis of SiO_2-supported Au nanoparticles decorated with small ($Ti_xSi_{1-x}O_2$) clusters (i.e. ($Ti_xSi_{1-x}O_2$)/[Au/SiO_2] used a polymethylhydrosiloxane oligomer modified with amine and Ti complex (PMHS-TiO_x). They were prepared by forming Au-amine complexes using amine-functionalized PMHS-TiO_x,[13] followed by reduction to form colloidal Au nanoparticles in close proximity to the isolated TiO_x units in a shell of PMHS-TiO_x.[14] Subsequent deposition of this Au-PMHS-TiO_x onto silica followed by low temperature oxidation to remove organics generated ($Ti_xSi_{1-x}O_2$)/[Au/SiO_2]. When they were used in the probe reaction of selective oxidation of C_3H_8 in a stream of O_2 and H_2, their catalytic properties were found to be highly sensitive to the presence of TiO_x surrounding the Au. The hydrocarbon product selectivity over ($Ti_xSi_{1-x}O_2$)/[Au/SiO_2] was exclusively acetone whereas over Au/TiO_2 it was predominantly C_3H_6. Furthermore, coating Au/TiO_2 with TiO_x-SiO_2 switched the product selectivity towards acetone.[15] These interesting catalytic data and the ubiquitous presence of metal-support oxide interface in heterogeneous catalysts suggest that further investigation is warranted, especially if the catalytic data can be complemented with detailed characterization of the Ti-oxo clusters. In addition, the use of better defined precursors than the flexible PMHS-TiO_x oligomer, which contained multiple TiO_x units within each chain, may aid in developing a better understanding towards controlled generation of well-defined metal-support oxide interfaces. Other researchers have attempted to form well-defined oxometal centers in a silica matrix. Tilley and coworkers used the thermolytic molecular precursor (TMP) approach.[16] However, calcination at high temperature of the material could lead to crystalline domains of metal oxide in silica.[17] Co-thermolysis of the TMP precursor with tris(*tert*-butoxy)silanol indicated that formation of the segregated oxide phase was only suppressed at high Si:M ratio.[18] Grafting of TMP onto high surface area mesoporous silica resulted in high retention of isolated metal centers, but oligomerization of the oxometal species still occurred upon calcination.[19] Thus, understanding factors that could influence the extent of agglomeration of the species is advantageous. Furthermore, TMPs studied were generally metal alkoxysiloxy complexes[16] which would not preferentially adsorb onto metal nanoparticles.

In this study, we aimed to explore precursors suitable for modification of metal particle surfaces that would interact strongly with but without poisoning the metal particles. We designed and synthesized a mononuclear Ti complex which contains two pyridylsiloxane ligands, $Ti(acac)_2[OSiC_6H_5N(OCH_3)_2]_2$ **III**.

Since it is known that molecules with multiple pyridyl units interact strongly with Au surfaces,[20] the two pyridyl units are expected to act like chelates with the Au surface. After mild oxidation to remove the organics, the resulting TiO_x will be flanked by two SiO_x units to form ($Ti_xSi_{1-x}O_2$) clusters that decorate the Au surface. Two methods of preparing the decorated Au/SiO_2 were examined. In method A, a calcined Au/SiO_2 that was pre-modified by silylation to cover the exposed SiO_2 surface was exposed to **III** by impregnation. In method B, colloidal Au particles were first formed by reducing a Au salt in solution in the presence of **III**. Then the **III**-encapsulated Au colloid was deposited onto SiO_2. Characterization of these samples with DR-UV-Vis, XPS and XAS showed differences in the structure of the ($Ti_xSi_{1-x}O_2$) coatings, which also led to different behavior in the catalytic selective oxidation of propane.

II. Experimental

II.A Synthesis of inverse catalyst ($Ti_xSi_{1-x}O_2$)/[Au/SiO_2]

The source and purity of all chemicals purchased are listed in Electronic Supplementary Material (ESM). Scheme 1 shows the steps in the synthesis of the Ti complex ligand **III**. 3-Pyridyldimethylsilane **I** and 3-pyridyldimethylsilanol **II** were prepared using published procedures.[21] Their NMR spectra are shown in ESM Figure S-1 and Figure S-2, respectively. For comparison, a Au/TiO_2 was prepared by deposition-precipitation at pH 7 and 70 °C using $HAuCl_4$ as the Au precursor and titania P25 as the support. The resulting powder was calcined in air at 400 °C (2 °C/min ramp) for 4 h. Details of the preparation of these samples are in ESM.

To prepare compound **III**, titanium diisopropoxide (bis-2, 4-pentanedionate) (2 mmol as 0.49 mL 75% isopropanol solution) was added over 1 min using a syringe into a N_2-purged flask containing 5 mmol **II** in 40 mL ether. After 60 min stirring at room temperature, **III** was recovered as a viscous light yellow liquid after solvent removal under 50 mtorr pressure. Yield: 90%, with less than 10% of the disiloxane present as a contaminant, as judged by ^{1}H NMR (ESM Figure S-3). ^{1}H NMR (400 MHz, $CDCl_3$): δ 8.74 (bs, 1H), 8.54 (dd, 1H), 7.94 (dt, 1H), 7.21 (ddd, 1H), 5.53 (bs, 1H), 1.96 (d, 6H) ppm, 0.31 (s, 6H) ppm. ^{13}C NMR (100 MHz, $CDCl_3$): δ 192.00, 189.42, 186.67, 153.89, 149.53, 141.29, 135.57, 122.75, 103.80, 25.59, 25.16, 0.65 ppm. ^{29}Si NMR (80 MHz, $CDCl_3$): δ -0.5 ppm.

Two methods, shown in Scheme 2, were used to prepare inverse catalysts labelled A- and B-$Ti_n/[Au/SiO_2]$, according to whether method A or B was used, and the number n corresponded to the Ti weight loading. The Au loading was around 1 wt% for all samples. In Method A, a Au/SiO_2 catalyst was first prepared with the aid of amine functionalized PMHS and calcined in a procedure similar to that published previously.[14] After calcination, it was silylated with hexamethyldisilazane. While under flowing N_2, 3 g of this silylated Au/SiO_2 was added to 40 mL THF, followed by **III**. After stirring overnight in the dark, the solution was dried under vacuum, and then in flowing He at 130 °C. The resulting solid was treated with a stream of O_3/O_2 mixture at 120 °C to oxidize the organics. After washing the solid to remove

chloride impurities, it was heated again in a O_3/O_2 stream slowly to 150 °C for 2 h. Four samples were prepared: A-Ti_0/[Au/SiO_2] (a control sample containing no Ti), A-$Ti_{1.3}$/[Au/SiO_2], A-$Ti_{1.9}$/[Au/SiO_2] and A-$Ti_{2.5}$/[Au/SiO_2].

For method B, a Au colloid was first prepared by mixing (tetrahydrothiophene)gold(I)chloride (Au(THT)Cl) with **III** in THF under N_2 in the dark. The amount of **III** used corresponded to a pyridyl to Au molar ratio of 10, 20, and 30 for samples B-$Ti_{1.3}$/[Au/SiO_2], B- $Ti_{2.5}$/[Au/SiO_2], and B-$Ti_{3.8}$/[Au/SiO_2], respectively. Triethylsilane (-SiH to Au molar ratio of 3, diluted in THF) was added to reduce the Au. The resulting colloidal suspension was impregnated onto Cab-O-Sil-L-90 to generate the samples after calcination and washing as described for the samples in method A.

II.B Characterization

NMR spectra were recorded with an Agilent DD2 spectrometer, operated at 400 MHz for ^1H, 100 MHz for ^{13}C, and 79 MHz for ^{29}Si. Spectra of moisture sensitive compounds were recorded in sealed J. Young NMR tubes. The ^1H and ^{13}C NMR chemical shifts, reported relative to $SiMe_4$, were determined by secondary references to the residual ^1H and ^{13}C peak of the deuterated solvent resonances. ^{29}Si NMR chemical shifts were referenced to TMS at 0.0 ppm. All the NMR data were processed and analyzed by MNova 9.0 software. High angle annular dark field (HAADF) STEM images were obtained using a JEOL 2100-F transmission electron microscope with a field emission gun at 200 kV, which has a spatial resolution of 0.2 nm. Particle size analyses were performed using the program Image J. The samples were suspended in ethanol and dried onto a 400 mesh copper grid with holey carbon or ultrathin carbon film (Ted Pella) for analysis.

The Brunauer-Emmett-Teller (BET) surface areas were determined with Micromeritics ASAP 2010 absorptometer. Inductively coupling plasma (ICP-OES) analysis to determine metal loading was conducted using a Varian Vista MPX ICP-OES. The samples were digested with a solution containing a mixture of concentrated hydrofluoric acid, nitric acid, and hydrochloric acid and then diluted to metal concentrations of 5-10 ppm. Standards for Ti and Au were prepared from 1000 mg/L ICP standard solutions from Sigma-Aldrich Co, LLC.

X-ray photoelectron spectroscopy (XPS) was performed using a Thermo ESCALAB 250Xi equipped with an electron flood gun, using AlK_α radiation (1486.6 eV) and adventitious carbon (1s) as reference. Diffuse reflectance ultraviolet-visible (DR-UV-Vis) measurements were performed on a Perkin Elmer Lambda 1050 spectrophotometer with an integration sphere. Silylated silica was used to collect baselines in these measurements.

X-ray absorption (XAS) spectroscopy was performed at beamline 5-BMD of the Dupont-Northwestern-Dow Collaborative Access Team (DND-CAT) located in the Advanced Photon

Source, Argonne National Laboratory, using the fluorescence mode. The Au L_{III} edge data were collected with the sample in the ambient, whereas the Ti K edge data were collected at room temperature in He using a custom sample holder that allowed pretreatment with a flow of He at 300 mL min^{-1} at 120 ℃ for 30 min. TS-1, pretreated in He at 180 ℃ for 1 h, and TiO_2 anatase in the ambient were used as standards. XAS data were analyzed by a package software, Demeter. [22] The Ti pre-edge features were fitted with four Gaussian peaks denoted as A1, A2, A3 and B with an arctan function as the baseline. Theoretical models from Atoms.inp Archive were used for EXAFS fitting.[23]

II.C Catalytic Tests

Selective oxidation of propane was performed in a packed bed reactor from 180 to 220 ℃ under atmospheric pressure, using 150 mg of catalyst, a feed of C_3H_8: O_2: H_2: He of a volumetric ratio of 5: 5: 5: 85, and a space-velocity of 5100 cm^3 h^{-1} $gcat^{-1}$ (30 mL min^{-1}). The catalysts were activated at 240 °C under reaction conditions until the products stabilized. Each reaction run lasted 3 h after stabilization, and each catalyst was tested in triplicate. The products were analyzed by on-line gas chromatography (Agilent 6890 GC with 5973 MSD) using two columns: a Porapak-Q (80/100 mesh) packed column for CO_2, H_2O, propane, propene, and acetaldehyde, and a Econo-cap EC-Wax capillary column for acetaldehyde, isopropanol, acetone, and other C_2-C_3 oxygenates.

Conversions and selectivities were calculated using these formulae. Conversion = (Σ_i (N_i/3) mol oxygenate i + (1/3) mol CO_2)/(mol of C_3H_8 in feed); Selectivity for CO_2 = (mol CO_2/3)/[Σ_i (N_i/3) mol oxygenate i + (1/3) mol CO_2]; Selectivity for oxygenate i = ((N_i/3) mol oxygenate i)/[Σ_i (N_i/3) mol oxygenate i + (1/3) mol CO_2]. Here N_i is the number of carbon atoms in product i.

III. Results and Discussion

III.A Structure of Inverse Ti_x/[Au/SiO_2]catalysts

The complexing Ti ligand was prepared according to Scheme 1. The scheme was based on our previous experience in synthesizing **I** and **II**.[21] These compounds were stored as dilute solutions to prevent **II** from self-condensation. Upon addition of titanium diisopropoxide (bis-2,4-pentanedionate) to **II**, heterofunction condensation between the isopropoxide groups of Ti and silanol was rapid and **III** was formed at room temperature in good yield in 1 h.

Since silica is regarded as an inert support and Au/SiO_2 showed negligible activity for propane oxidation under our reaction conditions,[14] catalytic differences in the samples in this study should stem from the different Au-TiO_x interfacial perimeter sites generated consequent of the different preparation procedures shown in Scheme 2. The procedural difference between the two methods was whether the Au particles were first formed and deposited on SiO_2 before being

decorated (Method A), or being decorated as they were formed in solution (Method B). In both preparation methods, the Ti/Au atomic ratio ranged from ~0.3 to ~1. Considering a metal dispersion of ~0.2, we expected high coverages of the Au particles. Inevitably there would be $Ti_xSi_{1-x}O_2$ deposition on SiO_2, but these deposits on SiO_2 were determined to be catalytically inactive, *vide infra*, which was expected based on observations with bulk TiO_2.

III.A.1Nature of Au nanoparticles

There were no detectable Cl, N or S by XPS in any of the samples. For all Au containing samples, the XPS of the Au 4f spectra (Figure S-4) showed 2 broad peaks centered at 87.4 eV, corresponding to Au $4f_{7/2}$ and $Au4f_{5/2}$ of metallic Au. The peak intensities were all similar, consistent with their similar Au loadings. Au XANES spectra were all similar to that of Au foil and no intense white line characteristic of $Au(OH)_3$ was observed (Figure S-5a), confirming that the samples were completely reduced.

The Au EXAFS results (Figure S-5b and Table S-1) showed that the Au-Au bond lengths were 2.86-2.87 Å, which corresponded to Au particle sizes between 2.5 to 5 nm.[24] These values agreed reasonably well with the average Au particle sizes determined with STEM (Fig. 1 and Table 1). In general, the Au particle size increased with increasing Ti loading. The higher organic contents around the Au particles with increased Ti loading might result in more severe local heating during calcination and caused Au particle agglomeration. On the samples examined, there were no obvious changes in Au particle size or size distribution after reaction (Figure S-6).

The DR-UV-Vis spectra of the catalysts (Fig. 2) showed the characteristic Au plasmonic absorption from 524 to 540 nm.[25] A systematic difference in the plasmonic absorption bands was observed between the two preparation methods. For the A-series catalysts, the peak maxima and widths were similar to the parent Au/SiO_2 that **III** was deposited on. On the other hand, for the B-series samples the peak widths increased noticeably with increasing TiO_x loading, and there was a slight red shift of the peak maximum. The plasmonic resonance peak position was reported to depend only weakly on the Au particle size below 25 nm,[26] and the relatively unchanged peak positions observed were consistent with the small Au particle sizes for all our samples. In contrast, the peak width was reported to decrease with increasing Au particle size.[26] Claus et al.[27] observed that the full width at half-maximum (fwhm) decreased from 136 nm to 115 nm when the average diameter of Au increased from 1.1 nm to 5.3 nm. The A-series samples followed this trend; the fwhm of the plasmonic absorbance of $A\text{-}Ti_{2.5}/[Au/SiO_2]$ with larger Au particles was ~10% narrower than that of $A\text{-}Ti_{1.3}/[Au/SiO_2]$. In contrast, in spite of similar Au sizes as the A-series, the fwhm of the plasmonic peaks of the B-series samples were significantly wider, and they increased with increasing Ti loading. This trend of peak broadening at progressively higher TiO_x loading was opposite to the expected

dependence based on the Au particle size variation.[26] One explanation is that the change in peak width reflected heterogeneity in the surroundings of the Au nanoparticles in these samples. It is known that the peak position and fwhm of the Au plasmonic absorption is influenced by the dielectric function of the surrounding medium.[27-29] Thus the broad peak might be a superposition of multiple peaks of Au particles in somewhat different environments. One source of heterogeneity was the SiO_x-TiO_x moieties surrounding the Au nanoparticles in the B-series samples, as is discussed below.

III.A.2 Nature of the TiO_x species

For all samples, the observed XPS binding energies for Ti ranged from 458.8 eV to 459.3 eV and 464.6 eV to 465eV for the $2p_{3/2}$ and $2p_{1/2}$ transitions, respectively (Figure S-7).[30] These values were slightly higher than the 458.7 eV and 464.4 eV for Ti^{4+} in bulk TiO_2 (Figure S-7) but were lower than that of isolated tetrahedral Ti in TS-1 or Ti in highly siliceous matrix.[31] They were consistent with the DR-UV-vis peak positions, which fell between those of TS-1 and TiO_2, as well as the XANES pre-edge characterization that are described below.

The DR-UV-Vis absorption due to TiO_x showed a systematic red shift in the peak position at 200-350 nm with increasing Ti loading for both series A and B samples (Fig. 3). For small metal oxides domains, it is known that the band gap energy increases as the domain size decreases.[32] In the limit of isolated Ti in a hydrated TS-1, the absorption peak in the UV region was like that of a metal coordination complex, with a peak at ~225 nm (Fig. 3) that has been assigned to the ligand-to-metal charge transfer (CT) transition of octahedrally coordinated, isolated titanium atoms.[33] On the other hand, bulk anatase TiO_2 exhibited a broad band centered around 320 nm.[34] Thus, the systematic red shift of the peaks, while still at shorter wavelengths than for TiO_2, indicated formation of TiO_x clusters whose size increased with increasing Ti loading, possibly via formation of oligomerized Ti(IV) species,[34-36] although their domain sizes remained much smaller than bulk TiO_2. In general, the samples also showed broader absorption peaks than TS-1. These broad absorption peaks indicated a broad distribution of TiO_2 domain sizes in the samples, which extended to include isolated Ti as indicated by significant absorption at 225 nm for most of the samples. Judging from the wider peak widths and peaks at longer wavelengths, the B-series samples were less homogeneous and contained larger TiO_x domains than the A samples. We attributed this to the fact that in the reduction step to form Au nanoparticles in Method B, both Au(THT)Cl and **III** were present together. The HCl generated together with trace amounts of water present in the preparation mixture could hydrolyze the Si-O-Ti bonds in **III**, and the hydrolyzed TiO_x units could agglomerate. These resulted in the formation of a nonuniform shell of SiO_x-TiO_x around the Au nanoparticles. When the solution of these SiO_x-TiO_x-covered Au nanoparticles together with unhydrolyzed **III** was mixed with silica to form the supported catalysts, the moisture and silanol groups in silica further exacerbated the hydrolysis and

agglomeration. The end result was that most of the SiO_x-TiO_x oligomers formed porous shells around the Au particles, and some were deposited on silica. The presence of this heterogeneous, porous shell around the Au nanoparticles was reflected in the broad Au plasmonic resonance shown in Fig. 2.

It is important to note that in all samples, moles of Ti added were higher than moles of surface Au atoms. The excess **III** was added to partially compensate for the much larger surface area of SiO_2 than Au, in spite of the expected much stronger interaction of **III** with Au surface than the silylated SiO_2 surface. In method A, when **III** was added to Au/SiO_2, it adsorbed onto Au through the pyridyl groups. This mode of interaction together with excess **III** fostered high coverage of **III** on Au. Thus, the Au DR-UV spectra of all samples prepared with this method were similar. The differences in their Ti DR-UV spectra reflected changes in the distribution of the TiO_x species, some of which resided on the support, with increase in Ti loading. In method B, the Au nanoparticles were already surrounded by aggregates of partially hydrolyzed and agglomerated **III**, the thickness of which increased with Ti loading. After calcination, these resulted in overlayers of different thicknesses that contained TiO_x domains of different sizes. Thus, the immediate neighboring medium around Au was more heterogeneous, which led to broad Au plasmon peaks. Deduced from the Au plasmonic peak widths, the heterogeneity increased with increase in Ti loading.

Samples A-$Ti_{1.3}$/[Au/SiO_2], A-$Ti_{2.5}$/[Au/SiO_2], and B-$Ti_{2.5}$/[Au/SiO_2] were investigated with XAS. It has been shown by computational studies that at the Ti K-edge, the pre-edge peak of the 1s → 3(mixed p-d) or 3d transition depends sensitively on the Ti-O bond length, coordination, symmetry and distortion of the Ti.[37] Whereas the DR-UV data were collected under ambient conditions, the XAS data were collected under He flow at room temperature after pretreatment at 120 ^oC, and they provided information not affected by exposure to ambient atmosphere.

The Ti pre-edge structures of TS-1, anatase, A-$Ti_{1.3}$/[Au/SiO_2], A-$Ti_{2.5}$/[Au/SiO_2], and B-$Ti_{2.5}$/[Au/SiO_2] are shown in Figure S-9. The $^{[4]}$Ti in TS-1 exhibited a single, intense pre-edge feature at 4969.6 eV, whereas $^{[6]}$Ti in TiO_2 anatase showed a weak feature at 4971.6 eV. The pre-edge structures of A-$Ti_{1.3}$/[Au/SiO_2]and A-$Ti_{2.5}$/[Au/SiO_2] were similar to that of TS-1 but for the reduced intensity. The structure for B-$Ti_{2.5}$/[Au/SiO_2], although still mostly resembled that of TS-1, began to showed weak features of anatase. This trend was also manifested in the post-edge structures between 4980-5020 eV that also indicated the presence of smaller TiO_x clusters and/or disordered materials in the Ti_x/[Au/SiO_2] samples.[38]

Farges, et. al.[39] observed that the pre-edge peak intensity as well as peak position were highly indicative of the Ti coordination and the degree of disorder of the environment around it. Using an extensive list of Ti-containing oxides, they generated an empirical plot (Figure S-10) of normalized height versus energy position for Ti in 4-, 5- or 6-fold coordination. The pre-edge peak intensity decreased and shifted to higher energy with increasing coordination number. They also further concluded that using pre-edge energy

or normalized peak intensity alone could result in under-estimation and over-estimation of the co-ordination number. The observed pre-edge peak energy and intensity for three of our samples and the standards TS-1 and anatase were added to the data of Farges et al. and plotted in Figure S-10. Whereas the energy for all three $Ti_x/[Au/SiO_2]$ samples fell in between those characteristic of $^{[4]}Ti$ and $^{[5]}Ti$, their intensities were significantly lower than for typical $^{[4]}Ti$. Furthermore, the energies for the two samples prepared by Method A were lower than the one by Method B. We believe that the Ti in these samples existed in at least two different coordination states, probably a mixture of $^{[4]}Ti$ and $^{[6]}Ti$.

More information could be gained by deconvolution of the prominent features in the pre-edge region of the $Ti_x/[Au/SiO_2]$ samples, which could be fitted with 4 peaks assigned A_1, A_2, A_3 and B (Figure S-11).[40] The A_1, A_2, A_3 peaks originate from the transitions of Ti 1s to hybridized 3d-4p states, and the B peak is from 1s to hybridized 4p-4s. Notestein, et al.[41, 42] assessed Ti coordination by defining a sharpness parameter as the combined areas of A_2+A_3 transitions. They used this parameter and the area-averaged pre-edge energy of A_2 and A_3 fitted peaks as a measure of the availability of the 3d orbitals. Using compounds of known Ti coordination they observed a linear relationship between the area quantity $(A_2+A_3)/A_T$ and the weighted average pre-edge energy. For our samples, this quantity varied in the order: $A\text{-}Ti_{1.3}/[Au/SiO_2]$ > $A\text{-}Ti_{2.5}/[Au/SiO_2]$ (4) > $B\text{-}Ti_{2.5}/[Au/SiO_2]$. Applying Notestein's correlation to our samples, as shown in Fig. 4, the three $Ti_x/[Au/SiO_2]$ samples fell between those of 4-coordinated TS-1 and 5-coordinated fresnoite, consistent with the earlier conclusion of the presence of a mixture of coordination states, in agreement with the UV-vis spectral data.

III.B Catalytic propane oxidation

Table 1 summarizes the catalytic results. Au/SiO_2 was rather inactive with a barely measurable propane conversion of 0.07%. Similarly, little reaction was observed over the SiO_2 support alone, anatase, or calcined SiO_2 with deposited complex **III** (4 wt% Ti). The catalytic activities were much higher with samples containing both Au and TiO_x. These observations are consistent with the generation of Au and TiO_x interfaces by designed placement of **III** in proximity of Au nanoparticles and validated the use of this reaction as a suitable probe of interfacial site properties. The A-series samples showed similar turnover frequencies (TOFs) and this similarity indicated that at the lowest Ti loading of 1.3 wt.% the Au surface was already fully covered with TiO_x, and attested to the effectiveness of **III** in adsorbing onto the Au surface. The TOFs were lower than for samples prepared with method B as in the latter case, the whole Au colloidal particle was available for interaction with **III**.

The C_3H_8 oxidation probe reaction also showed that the product selectivity was highly sensitive to the nature of TiO_x moieties around the Au nanoparticles. The A series of catalysts exhibited exclusive hydrocarbon product selectivity for acetone. This dominance of acetone selectivity and

absence of propene was similar to that observed by the group of Oyama over Au/TS-1 catalyst where Ti existed as isolated TiO_x surrounded by siliceous units,[43] and on $(Ti_xSi_{1-x}O_2)/[Au/SiO_2]$ prepared with Ti complex-modified polymethylhydrosiloxane oligomers.[14, 15, 44] The similarities in the TOFs and product selectivities among samples in this series paralleled the similarity in their Au DR-UV spectra, which showed rather narrow peaks indicating that the environment of Au was rather homogeneous. On these samples, in addition to the isolated TiO_x species decorating the Au particles, there was also a significant fraction of TiO_x deposited on the support not associated with Au. This population of TiO_x was oligomeric in nature, and its density increased with increasing Ti loading and probably contributed to the increased production of CO_2, since we observed that acetone reacted over Au/TiO_2, yielding 95% CO_2 and 5% acetaldehyde at ~10% conversion.

The differences between the A- and B-series of samples were striking, and their magnitude grew at progressively higher Ti loadings. The most prominent difference was the production of propene by the B-series where none was formed by the A-series. Spectroscopic characterizations of the B-series samples indicated that the surroundings of the Au nanoparticles were more heterogeneous (Fig. 2) and the TiO_2 domains were larger (Fig. 3) than the A-series samples, and these differences became increasingly prominent at higher Ti loadings. In other words, the TiO_x species that decorated the B-series was more similar to bulk TiO_2 than those that decorated the A-series, with the latter being closer to the isolated Ti in TS-1. This explains the production of propene from the B-series, since Au/TiO_2 produces propene (and CO_x) with very little acetone.[15, 43]

IV. Conclusions

TiO_x clusters were successfully deposited onto Au nanoparticles supported on SiO_2, where the Ti coordination was lower than octahedral as indicated by pre-edge XANES and DR-UV-Vis, using low temperature routes involving complex **III**. For samples prepared with method A, some aggregation of TiO_x upon calcination took place but this primarily occurred at sites distant from the Au nanoparticles. This conclusion was based on acetone being the exclusive hydrocarbon product in selective C_3H_8 oxidation, similar to the isolated TiO_x centres in Au/TS-1 catalysts. In addition, the similarity of the FWHM of Au plasmon peaks attested to the homogeneity of environment around Au. Method B resulted in higher overall heterogeneity of TiO_x moieties as seen by pre-edge XANES and DR-UV-Vis. The broader FWHM of Au plasmon peak together with mixed hydrocarbon products of propene and acetone in selective C_3H_8 oxidation also pointed to greater inhomogeneity of the TiO_x units surrounding Au.

An advantage of method A lies in the prevention of premature hydrolysis of SiO-TiO_x heterolinkages. The retention of primarily isolated Ti centres around Au indicates that method A is suitable to be used for other oxo metal clusters-decorated Au catalysts, since the central Ti atom in **III** can readily be substituted with Zr, Hf or Sn. Conversely, instead of Au nanoparticles, other metallic nanoparticles can be decorated. Thus, the method can be applied to synthesis of other uniform metal oxo clusters around metal nanoparticles. The underlying concept is to identify and utilize appropriate interaction of rationally designed metal oxo cluster precursors with metal nanoparticle. It is versatile, and offers high molecular control in the formation of inverse metal-metal oxide catalysts.

Acknowledgements

The authors acknowledge support of this work by the U.S. Department of Energy, Office of Science, Office of Basic Energy Sciences under Award Number DOE DE-FG02-03-ER15457. Linping Qian for experimental assistance, China Scholarship Council for support of Z.W. and X. H. This work made use of the EPIC, Keck-II, and/or SPID facility(ies) of Northwestern University's NUANCE Center, which has received support from the Soft and Hybrid Nanotechnology Experimental (SHyNE) Resource (NSF ECCS-1542205), the MRSEC program (NSF DMR-1121262) at the Materials Research Center, the International Institute for Nanotechnology (IIN), the Keck Foundation, and the State of Illinois, through the IIN. XRD patterns were collected in the J.B. Cohen X-Ray Diffraction Facility supported by the MRSEC program of the National Science Foundation (DMR- 1121262) at the Materials Research Center of Northwestern University. XAS were collected at Sector 5 of the DuPont-Northwestern-Dow Collaborative Access Team (DND-CAT) at the Advanced Photon Source (APS). DND-CAT was sup- ported by Northwestern University, E.I. DuPont de Nemours & Co., and The Dow Chemical Company and the Advanced Photon Source is a U.S. Department of Energy (DOE) Office of Science User Facility operated for the DOE Office of Science by Argonne National Laboratory under Contract No. DE-AC02-06CH11357. The CleanCat Core facility was funded by in part by the U.S. Department of Energy (DE-FG02-03ER15457). We also thank the Cabot Corporation for the gift of Cab-O-Sil L-90.

References

[1] G. Bond, D. Thompson, Gold-catalysed oxidation of carbon monoxide, Gold Bull 33(2) (2000) 41-50.
[2] J.D. Henao, T. Caputo, J.H. Yang, M.C. Kung, H.H. Kung, In Situ Transient FTIR and XANES Studies of the Evolution of Surface Species in CO Oxidation on Au/TiO2, Journal of Physical Chemistry B 110(17) (2006) 8689-8700.
[3] S.M. Oxford, J.D. Henao, J.H. Yang, M.C. Kung, H.H. Kung, Understanding the effect of halide poisoning in CO oxidation over Au/TiO2, Applied Catalysis, A: General 339(2) (2008) 180-186.
[4] I.X. Green, W. Tang, M. Neurock, J.T. Yates, Jr., Spectroscopic Observation of Dual Catalytic Sites During Oxidation of CO on a Au/TiO2 Catalyst, Science (Washington, DC, U. S.) 333(Copyright (C) 2013 American Chemical Society (ACS). All Rights Reserved.) (2011) 736-739.
[5] J. Saavedra, H.A. Doan, C.J. Pursell, L.C. Grabow, B.D. Chandler, The critical role of water at the gold-titania interface in catalytic CO oxidation, Science 345 (2014) 1599-1602.
[6] A.F. Carley, D.J. Morgan, N. Song, M.W. Roberts, S.H. Taylor, J.K. Bartley, D.J. Willock, K.L. Howard, G.J. Hutchings, CO bond cleavage on supported nano-gold during low temperature oxidation, Physical chemistry chemical physics : PCCP 13(7) (2011) 2528-38.

[7] J. Saavedra, T. Whittaker, Z. Chen, C.J. Pursell, R.M. Rioux, B.D. Chandler, Controlling activity and selectivity using water in the Au-catalysed preferential oxidation of CO in H2, Nature Chemistry 8(6) (2016) 584-589.
[8] A. Ostroverkh, V. Johanek, P. Kus, R. Sediva, V. Matolin, Efficient Ceria-Platinum Inverse Catalyst for Partial Oxidation of Methanol, Langmuir 32(25) (2016) 6297-6309.
[9] W. Kudernatsch, G. Peng, H. Zeuthen, Y. Bai, L.R. Merte, L. Lammich, F. Besenbacher, M. Mavrikakis, S. Wendt, Direct Visualization of Catalytically Active Sites at the FeO-Pt(111) Interface, ACS Nano 9(8) (2015) 7804-7814.
[10] S.D. Senanayake, D. Stacchiola, J.A. Rodriguez, Unique Properties of Ceria Nanoparticles Supported on Metals: Novel Inverse Ceria/Copper Catalysts for CO Oxidation and the Water-Gas Shift Reaction, Accounts of Chemical Research 46(8) (2013) 1702-1711.
[11] A. Corma, P. Concepción, M. Boronat, M.J. Sabater, J. Navas, M.J. Yacaman, E. Larios, A. Posadas, M.A. López-Quintela, D. Buceta, E. Mendoza, G. Guilera, A. Mayoral, Exceptional oxidation activity with size-controlled supported gold clusters of low atomicity, Nat Chem 5(9) (2013) 775-781.
[12] M. Turner, V.B. Golovko, O.P.H. Vaughan, P. Abdulkin, A. Berenguer-Murcia, M.S. Tikhov, B.F.G. Johnson, R.M. Lambert, Selective oxidation with dioxygen by gold nanoparticle catalysts derived from 55-atom clusters, Nature 454(7207) (2008) 981-983.
[13] Z. Wang, E.V. Beletskiy, S. Lee, X. Hou, Y. Wu, T. Li, M.C. Kung, H.H. Kung, Amine-functionalized siloxane oligomer facilitated synthesis of subnanometer colloidal Au particles, Journal of Materials Chemistry A: Materials for Energy and Sustainability 3(4) (2015) 1743-1751.
[14] N.A. Mashayekhi, Y.Y. Wu, M.C. Kung, H.H. Kung, Metal nanoparticle catalysts decorated with metal oxide clusters, Chem Commun (Camb) 48(81) (2012) 10096-8.
[15] N.A. Mashayekhi, M.C. Kung, H.H. Kung, Selective oxidation of hydrocarbons on supported Au catalysts, Catalysis Today 238 (2014) 74-79.
[16] K.L. Fujdala, R.L. Brutchey, T.D. Tilley, Tailored oxide materials via thermolytic molecular precursor (TMP) methods, Topics in Organometallic Chemistry 16(Surface and Interfacial Organometallic Chemistry and Catalysis) (2005) 69-115.
[17] K.L. Fujdala, T.D. Tilley, New Vanadium Tris(tert-butoxy)siloxy Complexes and Their Thermolytic Conversions to Vanadia-Silica Materials, Chemistry of Materials 14(3) (2002) 1376-1384.
[18] J.P. Dombrowski, G.R. Johnson, A.T. Bell, T.D. Tilley, Ga[OSi(OtBu)3]3·THF, a thermolytic molecular precursor for high surface area gallium-containing silica materials of controlled dispersion and stoichiometry, Dalton Transactions 45(27) (2016) 11025-11034.
[19] J. Jarupatrakorn, T.D. Tilley, Silica-Supported, Single-Site Titanium Catalysts for Olefin Epoxidation. A Molecular Precursor Strategy for Control of Catalyst Structure, Journal of the American Chemical Society 124(28) (2002) 8380-8388.
[20] Y. Ie, T. Hirose, H. Nakamura, M. Kiguchi, N. Takagi, M. Kawai, Y. Aso, Nature of Electron Transport by Pyridine-Based Tripodal Anchors: Potential for Robust and Conductive Single-Molecule Junctions with Gold Electrodes, Journal of the American Chemical Society 133(9) (2011) 3014-3022.
[21] M.N. Missaghi, J.M. Galloway, H.H. Kung, Bis (pyridyl) siloxane oligomeric ligands for palladium (II) acetate: synthesis and binding properties, Organometallics 29(17) (2010) 3769-3779.
[22] B. Ravel, M. Newville, ATHENA, ARTEMIS, HEPHAESTUS: data analysis for X-ray absorption spectroscopy using IFEFFIT, Journal of Synchrotron Radiation 12 (2005) 537-541.
[23] M. Newville, Atoms.inp Archive: Crystallographic Data from GSECARS.
[24] J.T. Miller, A.J. Kropf, Y. Zha, J.R. Regalbuto, L. Delannoy, C. Louis, E. Bus, J.A. van Bokhoven, The effect of gold particle size on AuAu bond length and reactivity toward oxygen in supported catalysts, Journal of Catalysis 240(2) (2006) 222-234.
[25] M.M. Alvarez, J.T. Khoury, T.G. Schaaff, M.N. Shafigullin, I. Vezmar, R.L. Whetten, Optical Absorption Spectra of Nanocrystal Gold Molecules, J. Phys. Chem. B 101(19) (1997) 3706-3712.

[26] S. Link, M.A. El-Sayed, Size and Temperature Dependence of the Plasmon Absorption of Colloidal Gold Nanoparticles, J. Phys. Chem. B 103(21) (1999) 4212-4217.
[27] P. Claus, A. Brueckner, C. Mohr, H. Hofmeister, Supported Gold Nanoparticles from Quantum Dot to Mesoscopic Size Scale: Effect of Electronic and Structural Properties on Catalytic Hydrogenation of Conjugated Functional Groups, J. Am. Chem. Soc. 122(46) (2000) 11430-11439.
[28] S. Underwood, P. Mulvaney, Effect of the Solution Refractive Index on the Color of Gold Colloids, Langmuir 10(10) (1994) 3427-30.
[29] S.K. Ghosh, S. Nath, S. Kundu, K. Esumi, T. Pal, Solvent and Ligand Effects on the Localized Surface Plasmon Resonance (LSPR) of Gold Colloids, J. Phys. Chem. B 108(37) (2004) 13963-13971.
[30] H. Liu, W. Yang, Y. Ma, Y. Cao, J. Yao, J. Zhang, T. Hu, Synthesis and characterization of titania prepared by using a photoassisted sol-gel method, Langmuir 19(7) (2003) 3001-3005.
[31] T. Blasco, M.A. Camblor, A. Corma, J. Perez-Pariente, The state of Ti in titanoaluminosilicates isomorphous with zeolite β, J. Am. Chem. Soc. 115(25) (1993) 11806-13.
[32] R.S. Weber, Effect of local structure on the UV-visible absorption edges of molybdenum oxide clusters and supported molybdenum oxides, J. Catal. 151(2) (1995) 470-4.
[33] V.A. de la Pena O'Shea, M. Capel-Sanchez, G. Blanco-Brieva, J.M. Campos-Martin, J.L.G. Fierro, The usefulness of time-dependent density functional theory to describe the electronic spectra of Ti-containing catalysts, Angewandte Chemie, International Edition 42(47) (2003) 5851-5854.
[34] S. Klein, S. Thorimbert, W. Maier, Amorphous microporous titania–silica mixed oxides: preparation, characterization, and catalytic redox properties, Journal of Catalysis 163(2) (1996) 476-488.
[35] T. Blasco, A. Corma, M. Navarro, J.P. Pariente, Synthesis, characterization, and catalytic activity of Ti-MCM-41 structures, Journal of Catalysis 156(1) (1995) 65-74.
[36] J. Klaas, G. Schulz-Ekloff, N.I. Jaeger, UV-visible diffuse reflectance spectroscopy of zeolite-hosted mononuclear titanium oxide species, The Journal of Physical Chemistry B 101(8) (1997) 1305-1311.
[37] N. Jiang, D. Su, J.C.H. Spence, Determination of Ti coordination from pre-edge peaks in Ti K-edge XANES, Physical Review B: Condensed Matter and Materials Physics 76(21) (2007) 214117/1-214117/9.
[38] V. Schwartz, D.R. Mullins, W. Yan, H. Zhu, S. Dai, S.H. Overbury, Structural investigation of au catalysts on TiO2-SiO2 supports: Nature of the local structure of ti and au atoms by EXAFS and XANES, Journal of Physical Chemistry C 111(46) (2007) 17322-17332.
[39] F. Farges, G.E. Brown, J.J. Rehr, Ti K-edge XANES studies of Ti coordination and disorder in oxide compounds: Comparison between theory and experiment, Physical Review B 56(4) (1997) 1809-1819.
[40] Z.Y. Wu, G. Ouvrard, P. Gressier, C.R. Natoli, Ti and O K edges for titanium oxides by multiple scattering calculations: Comparison to XAS and EELS spectra, Physical Review B 55(16) (1997) 10382-10391.
[41] J.M. Notestein, L.R. Andrini, V.I. Kalchenko, F.G. Requejo, A. Katz, E. Iglesia, Structural Assessment and Catalytic Consequences of the Oxygen Coordination Environment in Grafted Ti−Calixarenes, Journal of the American Chemical Society 129(5) (2007) 1122-1131.
[42] T.R. Eaton, M.P. Campos, K.A. Gray, J.M. Notestein, Quantifying accessible sites and reactivity on titania–silica (photo)catalysts: Refining TOF calculations, Journal of Catalysis 309(0) (2014) 156-165.
[43] J.J. Bravo-Suarez, K.K. Bando, T. Fujitani, S.T. Oyama, Mechanistic study of propane selective oxidation with H2 and O2 on Au/TS-1, J. Catal. 257(1) (2008) 32-42.
[44] Y.Y. Wu, N.A. Mashayekhi, H.H. Kung, Au–metal oxide support interface as catalytic active sites, Catalysis Science & Technology 3(11) (2013) 2881-2891.

Schemes and figures

Scheme 1 Synthesis of 3-pyridyldimethylsilane **I**, 3-pyridyldimethylsilanol **II**, and compound **III**.

Scheme 2 Synthesis of inverse ($Ti_xSi_{1-x}O_2$)-decorated Au nanoparticles on SiO_2 using method A and method B.

Fig. 1 STEM images of 1: A-Ti_0/[Au/SiO_2], 2: A-$Ti_{1.3}$/[Au/SiO_2], 3: A-$Ti_{1.9}$/[Au/SiO_2], 4: A-$Ti_{2.5}$/[Au/SiO_2], 5: B-$Ti_{1.3}$/[Au/SiO_2], 6: B-$Ti_{2.5}$/[Au/SiO_2], and 7: B-$Ti_{3.8}$/[Au/SiO_2]. Scale bar is 20 nm.

Fig. 2 Au plasmonic peak of: 1. A-Ti_0/[Au/SiO_2], 2. A-$Ti_{1.3}$/[Au/SiO_2], 3. A-$Ti_{1.9}$/[Au/SiO_2], 4. A-$Ti_{2.5}$/[Au/SiO_2], 5. B-$Ti_{1.3}$/[Au/SiO_2], 6. B-$Ti_{2.5}$/[Au/SiO_2], and 7. B-$Ti_{3.8}$/[Au/SiO_2]. Spectra are shifted vertically for clarity.

Fig. 3 DR-UV spectra of samples compared with TS-1 (dot-dash) and TiO_2 (dash).

Fig. 4 The relative area of peaks (A_2 and A_3)/A_T versus area-weighted average pre-edge energy, determined by the positions of A_2 and A_3. Red: TS-1; Green: anatase (this study); Blue: A-$Ti_{1.3}$/[Au/SiO_2] (2), A-$Ti_{2.5}$/[Au/SiO_2] (4), and B-$Ti_{2.5}$/[Au/SiO_2] (6). Other points are 4 co-ordinated Ba_2TiO_4 (open circle), 5 co-ordinated fresnoite (grey) and 6-co-ordinated anatase (black) taken from Todd, et al.[42] A_T is the total area of pre-edge peaks ($A_T=A_1 + A_2 + A_3 + A_B$).

Table 1 Selective oxidation of propane over gold catalysts.

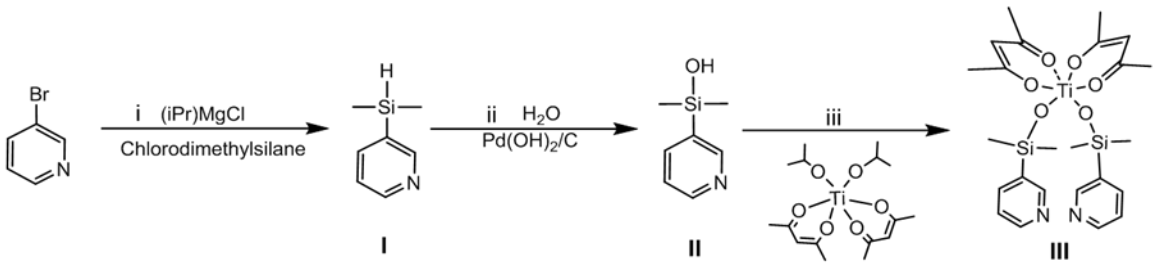

Scheme 1 Synthesis of 3-pyridyldimethylsilane **I**, 3-pyridyldimethylsilanol **II**, and compound **III**.

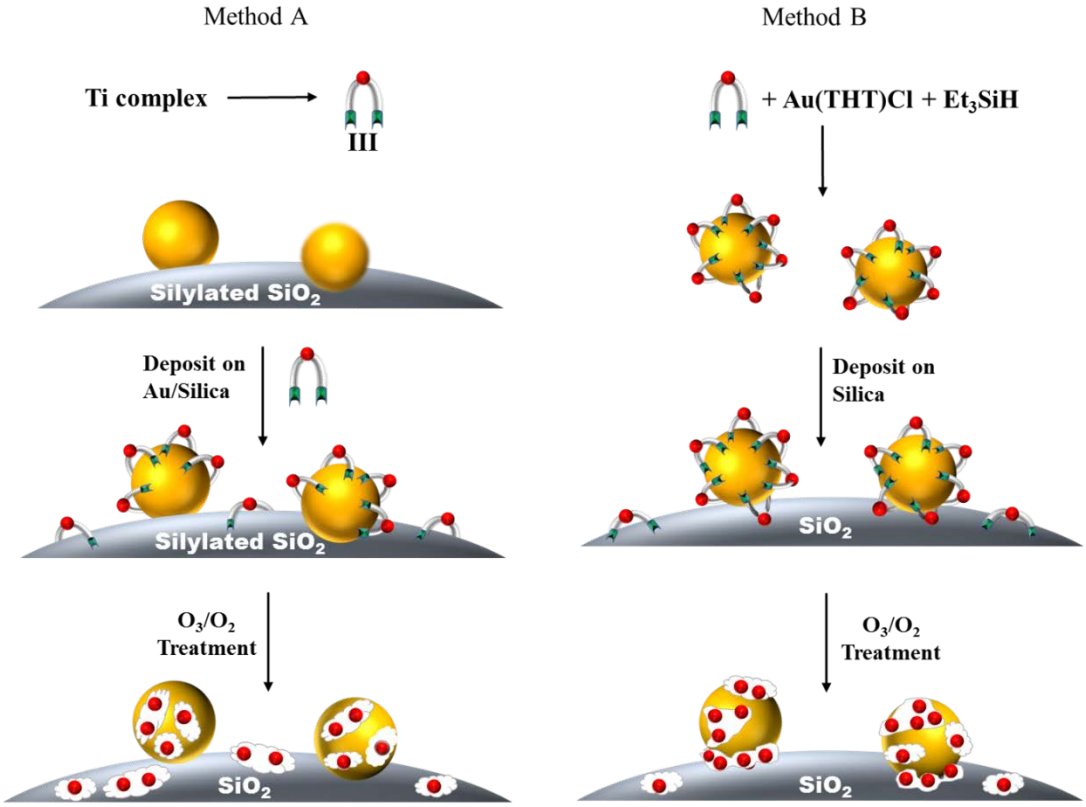

Scheme 2 Synthesis of inverse ($Ti_xSi_{1-x}O_2$)-decorated Au nanoparticles on SiO_2 using method A and method B.

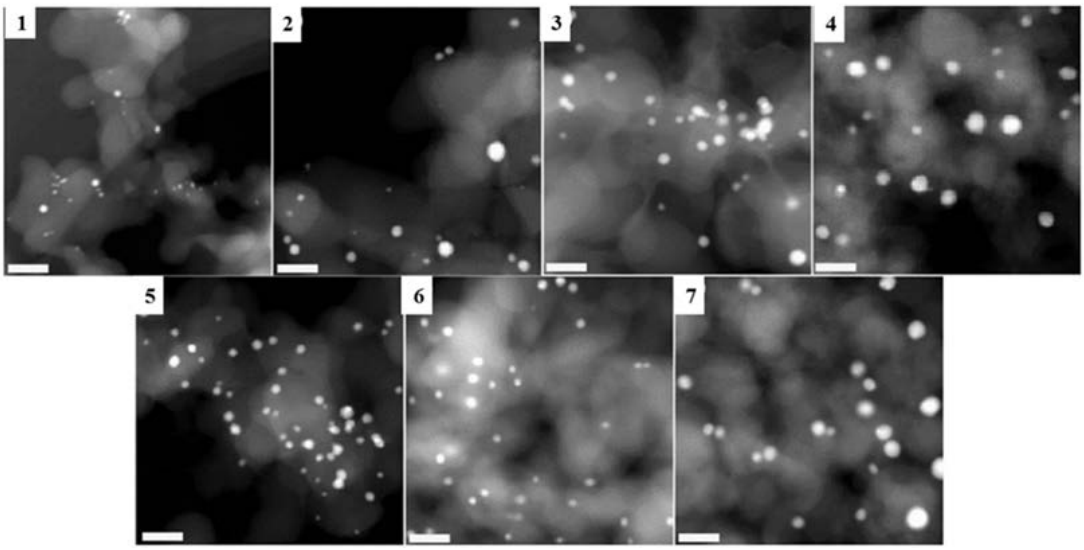

Fig. 1 STEM images of 1: A-Ti_0/[Au/SiO_2], 2: A-$Ti_{1.3}$/[Au/SiO_2], 3: A-$Ti_{1.9}$/[Au/SiO_2], 4: A-$Ti_{2.5}$/[Au/SiO_2], 5: B-$Ti_{1.3}$/[Au/SiO_2], 6: B-$Ti_{2.5}$/[Au/SiO_2], and 7: B-$Ti_{3.8}$/[Au/SiO_2]. Scale bar is 20 nm.

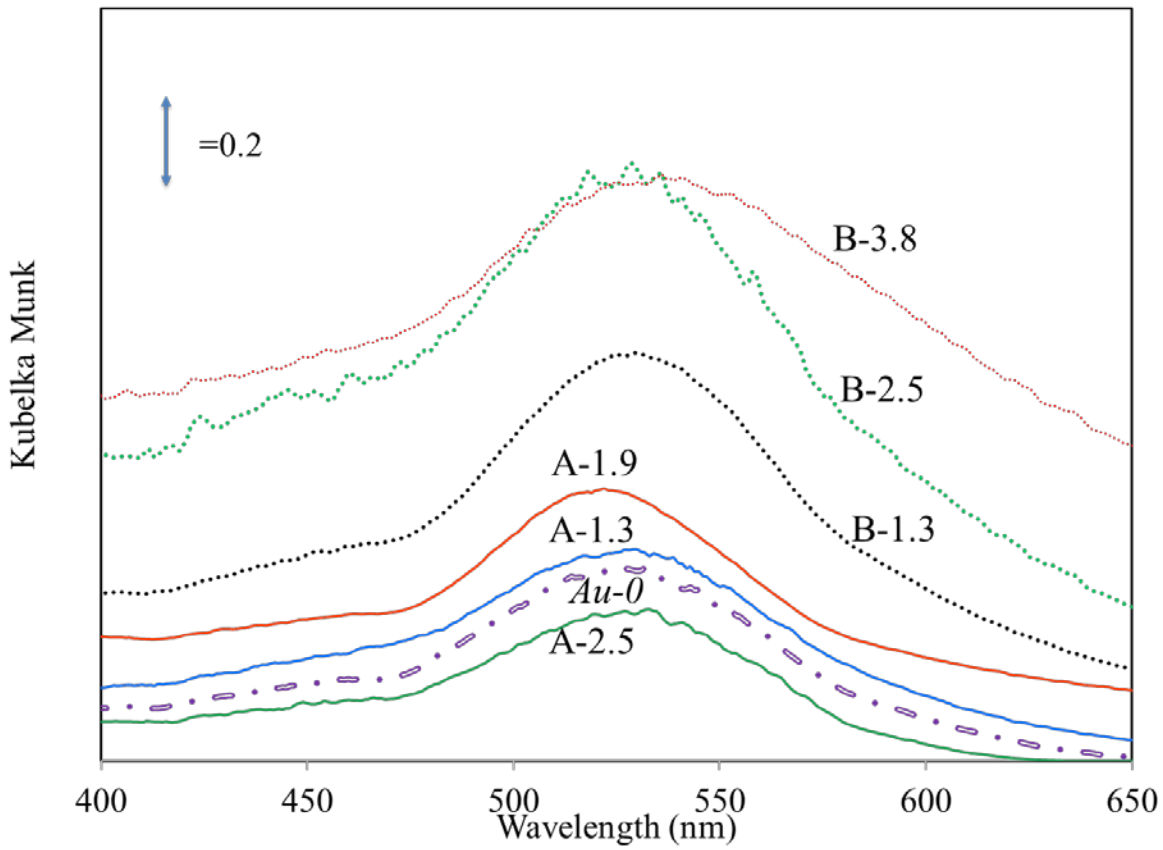

Fig. 2 Au plasmonic peak of A- and B-Ti_x/[Au/SiO_2]. Spectra are shifted vertically for clarity.

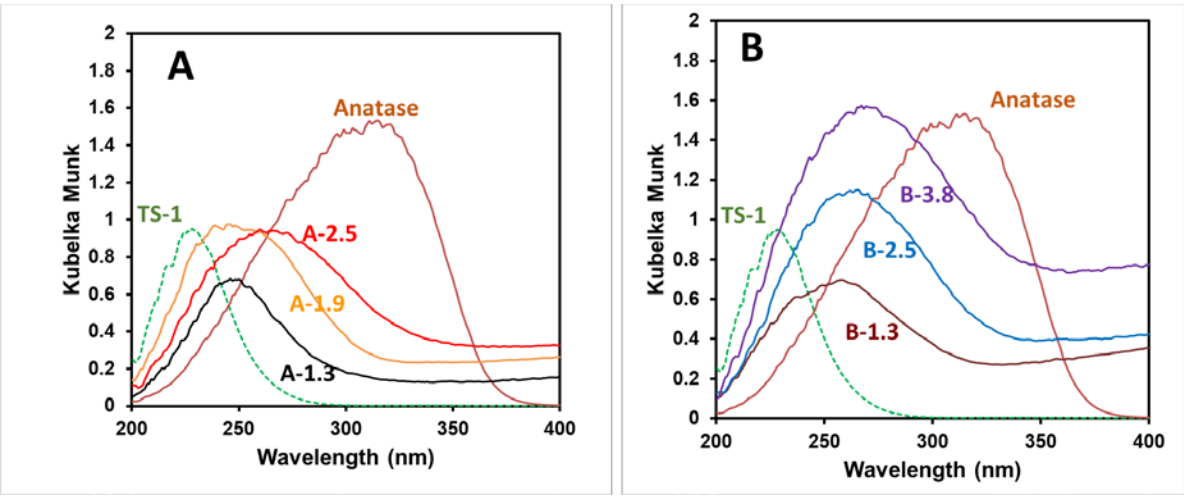

Fig. 3 DR-UV spectra of samples compared with TS-1 (dot-dash) and TiO_2 (dash).

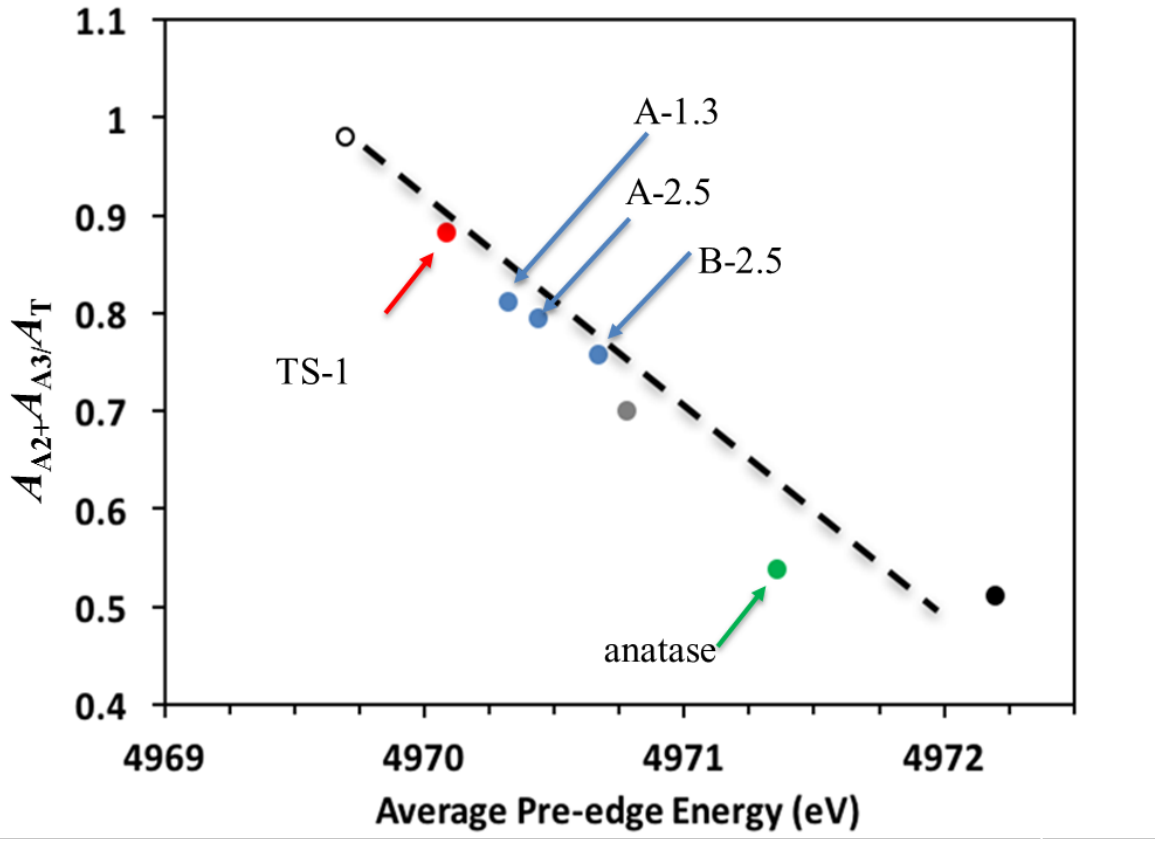

Fig. 4 The relative area of peaks (A_2 and A_3)/A_T versus area-weighted average pre-edge energy, determined by the positions of A_2 and A_3. 4 co-ordinated Ba_2TiO_4 (open circle), 5 co-ordinated fresnoite (grey) and 6-co-ordinated anatase (black) taken from Todd, et al.[42] A_T is the total area of pre-edge peaks ($A_T=A_{A1} + A_{A2} + A_{A3} + A_B$).

Table 1 Selective oxidation of propane over supported Au catalysts.

Sample	Au Dp[a] (nm)	Conv % C_3H_8	Selectivity %					TOF[b]	BET (m^2 g^{-1})
			C_3H_6O	C_3H_6	C_3H_7OH	C_2H_4O	CO_2		
A-Ti_0/[Au/SiO_2]	1.9 ± 0.6	0.07	68	0	5	0	28	0.36	68
A-$Ti_{1.3}$/[Au/SiO_2]	2.8 ± 2.0	1.05	92	0	2	0	6	8.5	88
A-$Ti_{1.9}$/[Au/SiO_2]	3.7 ± 1.6	0.86	80	0	3	0	17	9.0	84
A-$Ti_{2.5}$/[Au/SiO_2]	5.0 ± 2.1	0.65	73	0	2	0	25	9.1	75
B-$Ti_{1.3}$/[Au/SiO_2]	3.2 ± 2.0	1.30	50	27	3	5	15	11.7	83
B-$Ti_{2.5}$/[Au/SiO_2]	2.8 ± 0.9	1.65	46	33	4	7	10	12.8	91
B-$Ti_{3.8}$/[Au/SiO_2]	5.8 ± 2.8	1.01	40	41	2	9	8	16.3	80
Au/TiO_2	2.3 ± 0.6	0.90	4	65	0	0	26	5.8	80

Reaction conditions: Catalyst weight = 150 mg. C_3H_8:O_2:H_2: He = 5:5:5:85, total flow rate = 30 mL/min. Data shown were steady state results collected after 5 h time-on-stream at 240 °C. [a]Au average particle diameter Dp is calculated by 200 counts on STEM images. [b](mol $C_3H_{8converted}$) (mol $Au_{surface}$)$^{-1}h^{-1}$. Au dispersion calculated using the formula Dispersion = 1/Dp.